Electronic Structure of A- and B-Site Doped Lanthanum Manganites: A Combined X-ray Spectroscopic Study

K. Kuepper,*,† M. C. Falub,‡ K. C. Prince,§ V. R. Galakhov,|| I. O. Troyanchuk,⊥ S. G. Chiuzbaian,# M. Matteucci,⊗ D. Wett,○ R. Szargan,○ N. A. Ovechkina,|| Ya. M. Mukovskii,▽ and M. Neumann†

Department of Physics, University of Osnabrück, Barbarastr. 7, D-49069 Osnabrück, Germany; École Polytechnique Fédérale de Lausanne, IPN, Lausanne, CH-1015 Switzerland; Sincrotrone Trieste, km 163.5 in Area Science Park, I-34012 Basovizza (Trieste), Italy; Institute of Metal Physics, Russian Academy of Sciences−Ural Division, 620219 Yekaterinburg GSP-170, Russia; Institute of Solid State and Semiconductor Physics, National Academy of Sciences of Belarus, 220072 Minsk, Belarus; Paul Scherrer Institut, CH-5232 Villigen PSI, Switzerland; Institute of Condensed Matter, National Research Council, c/o Sincrotrone Trieste, in Area Science Park, Basovizza (Trieste), Italy; Wilhelm Ostwald Institute of Physical and Theoretical Chemistry, University of Leipzig, D-04103 Leipzig, Germany; and Moscow State Steel and Alloys Institute, 117936 Moscow, Russia

Received: December 7, 2004; In Final Form: March 22, 2005

The electronic properties of a series of colossal magnetoresistance (CMR) compounds, namely $LaMnO_3$, $La_{1-x}Ba_xMnO_3$ ($0.2 \leq x \leq 0.55$), $La_{0.76}Ba_{0.24}Mn_{0.84}Co_{0.16}O_3$, and $La_{0.76}Ba_{0.24}Mn_{0.78}Ni_{0.22}O_3$, have been investigated in a detailed spectroscopic study. A combination of X-ray photoelectron spectroscopy (XPS), X-ray emission spectroscopy (XES), X-ray absorption spectroscopy (XAS), and resonant inelastic X-ray scattering (RIXS) was used to reveal a detailed picture of the electronic structure in the presence of Ba, Co, and Ni doping in different concentrations. The results are compared with available theory. The valence band of $La_{1-x}Ba_xMnO_3$ ($0 \leq x \leq 0.55$) is dominated by La 5p, Mn 3d, and O 2p states, and strong hybridization between Mn 3d and O 2p states is present over the whole range of Ba concentrations. Co-doping at the Mn site leads to an increased occupancy of the e_g states near the Fermi energy and an increase in the XPS valence band intensity between 0.5 and 5 eV, whereas the Ni-doped sample shows a lower density of occupied states near the Fermi energy. The Ni d states are located in a band spanning the energy range of 1.5−5 eV. XAS spectra indicate that the hole doping leads to mixed Mn 3d−O 2p states. Furthermore, RIXS at the Mn L edge has been used to probe d−d transitions and charge-transfer excitations in $La_{1-x}Ba_xMnO_3$.

1. Introduction

The lanthanum manganese perovskites of the type $La_{1-x}A_xMnO_3$ (A = Ca, Sr, Ba) display a remarkably rich phase diagram as a function of temperature, magnetic field, and doping that is due to the intricate interplay of charge, spin, orbital, and lattice degrees of freedom. This competition of different phases on the nanoscale has been the subject of many studies during the past few years.[1−3] The variety of properties is often due to different behavior of 3d electrons, which may be more or less localized, giving rise to intraatomic correlation effects of varying strength. Moreover, they may either experience the orbital degeneracy compatible with a given crystal space group or lift this degeneracy, due to Jahn−Teller distortion. These types of behavior are to a large extent mediated by Mn 3d−O 2p hybridization, thus establishing a link to the chemistry of the compound in question. In a cubic crystal the Jahn−Teller distortion leads to a lowering of the symmetry and thus to a splitting of the e_g level. Its occupation, influenced by doping and energetic position, strongly influences the hybridization between the Mn 3d and the O 2p states, which is crucial for understanding the family of colossal magnetoresistance compounds. In the past few years, studies of these compounds were stimulated by the discovery of colossal magnetoresistance (CMR), a huge negative change in the electrical resistance induced by an applied magnetic field.[4,5] This behavior has been associated with half-metallic ferromagnetism, meaning that one spin channel is metallic while the other is insulating.[6,7] The spin-polarized Mn 3d electrons are the charge carriers.

$La_{1-x}Ba_xMnO_3$ is the first reported CMR model compound[4] with a Curie temperature of around 340 K.[8] The crystal structure changes from orthorhombic through rhombohedral ($x > 0.13$) to cubic ($x > 0.35$), and the system shows ferromagnetic behavior for Ba concentrations $x \geq 0.15$. It also undergoes a metal-to-insulator transition at $x \approx 0.20$.[8,9] This system has been subjected to intense investigation of its crystallographic and magnetic properties,[9,10] various phase transitions,[8,11,12] and spin dynamics[13] during the past few years. Also, the effect of Mn-site doping leads to remarkable magnetic transport phenomena since B-site doping with another 3d element such as Fe, Co, or Ni has a direct influence on the magnetic transport and exchange properties of the compound.[14] In particular, $La_{1-x}Ba_xMn_{1-y}Co_yO_3$

† University of Osnabrück.
‡ École Polytech Fédérale de Lausanne.
§ Sincrotrone Trieste.
|| Russian Academy of Sciences.
⊥ National Academy of Sciences of Belarus.
Paul Scherrer Institut.
⊗ Institute of Condensed Matter.
○ University of Leipzig.
▽ Moscow State Steel and Alloys Institute.
* Corresponding author: e-mail karsten.kuepper@uos.de.

10.1021/jp044447w CCC: $30.25
Published on Web 04/21/2005

is of interest since the Co substitution leads to a strong ferromagnetic $Mn^{4+}-O-Co^{2+}$ interaction. For single crystals of $La_{0.74}Ba_{0.26}Mn_{1-y}Co_yO_3$ it has been found that the Curie temperature decreases with increasing Co content, whereas the magnetoresistance shows sharp maxima, especially at a Co concentration of around 16%.[15] Recently some photoemission spectra of these compounds have been reported, revealing the divalent character of the Co ions in $La_{0.74}Ba_{0.26}Mn_{1-y}Co_yO_3$.[16,17] Nonetheless, in particular for the A- and B-site doped compounds, very few X-ray spectroscopic data are available up to now.

For the analysis of the spatial distribution of the electron density and chemical bonding the methods of X-ray and photoelectron spectroscopy provide a tool of unique precision, especially useful in combination with first-principles electronic structure studies. Several electronic structure studies have been reported, which nonetheless leave a number of essential questions unanswered. Several spectroscopic techniques, mostly X-ray photoelectron spectroscopy (XPS) and X-ray absorption spectroscopy (XAS), have been applied to $La_{1-x}A_xMnO_3$ (A = Ca, Sr).[18,19] Although the band structure of $LaMnO_3$ and $La_{1-x}A_xMnO_3$ (A = Ca, Sr, Ba) has been also studied theoretically by several local spin density approximation (LSDA) studies,[19−22] the importance and strength of correlation effects are still a controversial subject. For example, one of the most recent works comes to the conclusion that the stabilization of the cubic phase is more important for ferromagnetism in hole doped compounds than the double-exchange mechanism.[22]

Element and site specific resonant inelastic X-ray scattering (RIXS) spectroscopy[23,24] is also a powerful tool to investigate the electronic structure of transition metal compounds. XAS is the starting point for RIXS measurements since an excitation energy close to an absorption threshold leads to very different decay states than those at higher excitation energies (20−30 eV above the absorption edge), which instead results in normal X-ray emission spectroscopy (XES). This reflects the partial density of states which is symmetry-resolved by the dipole selection rules and broadened by the lifetime broadening. During resonant excitation an electron is promoted from a core state to (or just above) the Fermi energy. The emission features can be understood as being due to coherent elastic scattering and inelastic loss features which can be associated with the difference in energy between initial and final state. The RIXS cross section is described by the Kramers−Heisenberg equation.[25,26] The possibilities in the study of correlated systems by means of RIXS go from Coulomb interactions on high-energy scales over charge-transfer excitations to lower excitation energies, especially regarding optically inaccessible bands, such as d−d transitions.[27−29]

The 3d transition metal (TM) oxides belong to the most interesting materials for RIXS since the interpretation of the TM 2p → 3d → 2p RIXS data is controversial and highlights the limitations of both the band model and the Anderson impurity model. Butorin et al. reported RIXS spectra of MnO to be due to low-lying d−d and charge-transfer excitations, which can be described by an atomic multiplet calculation.[27] Furthermore, the Mn 2p → 3d → 2p RIXS spectra of $La_{0.5}Ca_{0.5}MnO_3$ have been interpreted within a charge-transfer multiplet approach.[30] On the other hand, Kurmaev et al. found that the effect of interatomic hybridization between Mn 3d and O 2p states is present over the whole valence band in $Pr_{0.5}Sr_{0.5}MnO_3$, leading to a more extended 3d wave function.[31] For this kind of system, RIXS leads to an observation of structural features in the occupied part of the valence band, and RIXS measures the joint DOS for vertical transitions.[31−33] Very recently, the Mn 2p → 3d → 2p RIXS in $La_{1-x}Na_xMnO_3$ has been interpreted as well in the band picture.[34]

We present here for the first time a detailed X-ray spectroscopic study of $La_{1-x}Ba_xMnO_3$ ($0.2 \le x \le 0.55$) and the mentioned A- and B-site doped manganites using a number of complementary spectroscopic techniques, namely XPS, XES, XAS, and RIXS. The results are analyzed with regard to the issues stated above, compared with measurements on undoped $LaMnO_3$, and discussed in the light of both available band structure calculations[20−22,35] as well as cluster model calculations.[27,36]

2. Experimental Details

High-quality $La_{1-x}Ba_xMnO_3$ ($0 \le x \le 0.55$) polycrystals were produced by solid-state reaction at the Moscow State Steel and Alloys Institute. X-ray analysis was used to check the structural quality and single phase nature of the specimens. $La_{0.76}Ba_{0.24}Mn_{0.84}Co_{0.16}O_3$ and $La_{0.76}Ba_{0.24}Mn_{0.78}Ni_{0.22}O_3$ single crystals were grown by the flux melt method.[15]

The XAS, XES, and RIXS data of $La_{1-x}Ba_xMnO_3$ were performed at room temperature at beamline 8.0.1 at the Advanced Light Source, Berkeley, using the X-ray fluorescence end station of the University of Tennessee at Knoxville.[37] Linearly polarized light with polarization in the horizontal plane was incident on the sample whose surface was in the vertical plane. Emission was measured along the electric vector of the incident light in the horizontal plane, that is, at a scattering angle of 90°. This geometry minimizes diffuse elastic scattering from the surface since the Brewster angle in the soft X-ray range is usually very close to 45° so that the reflectivity for $\vec{p}$ light is very close to zero. Photons with an energy of 520−670 eV are provided to the end station via a spherical 925 lines/mm grating monochromator. The Mn 3d → 2p and O 2p → 1s normal XES spectra were obtained with a 1500 lines/mm, 10 m radius grating. The excitation energies were set to 680 eV for the Mn L edge and to 600 eV for the O K edge. The overall resolution (beamline plus spectrometer) was set to around 1 eV. The overall resolution of the resonant excited Mn L emission spectra corresponds to the width of the elastic recombination peak at full width at half-maximum (fwhm), around 1 eV in the present case. The spectra were calibrated using a reference sample of pure Mn metal and MgO, respectively. The RIXS spectra recorded at the Mn L edge as well as the Mn 2p and O 1s X-ray absorption spectra were measured under the same experimental conditions in total electron yield mode. For the XAS experiments the instrumental resolution was set to 0.3 eV. Samples were scraped in air with a diamond file in order to reduce surface contamination just before mounting them in the transfer chamber. The XES spectroscopy on the $La_{0.76}Ba_{0.24}Mn_{0.84}Co_{0.16}O_3$ and $La_{0.76}Ba_{0.24}Mn_{0.78}Ni_{0.22}O_3$ single crystals was performed at the undulator based beamline ID12-2, using the rotatable spectrometer apparatus (ROSA) at BESSY II, Berlin. The excitation energies were set to 680 eV for the Mn L edge, to 850 eV for the Co L edge, to 900 eV for the Ni L edge, and to 600 eV for the O K edge, for both the measurements on the sample and the corresponding calibration spectra. The overall resolution (beamline plus spectrometer) was again set to around 1 eV.

XPS valence bands were recorded using a PHI 5600CI multitechnique spectrometer with monochromatic Al Kα ($h\nu$ = 1486.6 eV) radiation of 0.3 eV fwhm and with the sample at room temperature. The resolution of the analyzer is 1.5% of the pass energy, i.e., 0.35 eV, giving an overall resolution of

about 0.6 eV. All spectra were obtained using a 400 μm diameter analysis area. The samples were fractured in situ. The survey spectrum taken directly after breaking the samples shows only low contamination by hydrocarbons, and C 2p states should have no influence on the valence band spectra. The spectra were calibrated against the Au $f_{7/2}$ signal from an Au foil ($E_B = 84.0$ eV).[38] During all measurements, the pressure in the main chamber was kept below 1×10^{-9} mbar.

3. Results

3.1. XPS and XES. To study the influence of Ba-doping on the Mn 3d−O 2p hybridization we performed XES measurements on the Mn 2p and the O 1s edges of undoped $LaMnO_3$ and all of the Ba-doped compounds.

The results are shown in Figure 1. The Mn 2p and O 1s XES spectra and the theoretical results[22,21] have been plotted on a binding energy scale for comparison. The XES and valence band XPS spectra have been aligned on a common energy scale by subtracting the XES energies from the corresponding XPS core level binding energies. Hence, the XES spectra reflect the site-specific partial densities of states of the different elements in the compound which is symmetry-selected by the dipole selection rule and broadened by the core hole lifetime and the spectrometer resolution. The Mn 2p and O 1s XES spectra overlap in a large part of the valence band, indicating significant hybridization between Mn 3d and O 2p states. The valence band region consists of four distinct features labeled *a*−*d*, which, for the undoped $LaMnO_3$, are in excellent agreement with the theoretical results. From the Mn 2p XES spectra, band *a* just below the Fermi level can be attributed to Mn 3d states, and moreover theory reveals band *a* to be due to Mn e_g electrons.[22] Feature *b* is located at a binding energy of 2.5 eV and mainly formed by Mn t_{2g} states whereas band *c* around 4 eV can be associated with overlapping Mn 3d t_{2g} and O 2p states. Finally, feature *d* (∼6 eV) is composed of hybridized Mn 3d, O 2p, and La 5p bands. Doping with Ba^{2+} leads to a shift of features *b*−*d* toward the Fermi level. According to the calculations,[21,22] band *b* shifts from 2.5 eV in $LaMnO_3$ to around 1.8 eV in $La_{0.8}Ba_{0.2}MnO_3$ and to approximately 1.4 eV binding energy in $La_{0.60}Ba_{0.40}MnO_3$. Feature *c* moves closer to E_F from 4 eV in the valence band of $LaMnO_3$ to ∼3.6 eV in the case of $La_{0.8}Ba_{0.2}MnO_3$ and finally to around 3.2 eV at higher Ba concentration while for band *d* a slight shift from 6 eV ($LaMnO_3$) to 5.5 eV for the valence band of $La_{0.60}Ba_{0.40}MnO_3$ is predicted.[21] These shifts are also present in the experimental results. Feature *b* moves closer to the Fermi level from 2.5 eV binding energy in $LaMnO_3$ to 2 eV in the case of $La_{0.55}Ba_{0.45}MnO_3$, a smaller shift than the calculated one but detectable. The experimental data also reveal that feature *b* becomes broader with increasing doping concentration, which may indicate that the Mn t_{2g} states are somewhat less localized at higher hole concentration. In the case of feature *c* one can observe a shift from 4.5 to 3.5 eV at higher doping concentration ($x = 0.45, 0.55$). Also, band *d* shows a resolvable shift from around 6 eV ($LaMnO_3$) to 5.5 eV in the XPS valence band spectra for compounds with higher Ba concentrations. The Mn 3d → 2p XES spectra show a broad structure between the Fermi level and 5 eV comprising valence band features *a*−*c*. The maximum intensities of the O 2p → 1s XES spectra, mainly comprising band *c*, show a shift from 4.5 eV for $LaMnO_3$ to 3.5 eV, degenerate with the Mn t_{2g} states, for $La_{0.45}Ba_{0.55}MnO_3$.

Figure 2 displays the XPS valence band and the XES spectra of $La_{0.76}Ba_{0.24}Mn_{0.84}Co_{0.16}O_3$ and $La_{0.76}Ba_{0.24}Mn_{0.78}Ni_{0.22}O_3$, respectively. All spectra were normalized to the Ba 5p peak.

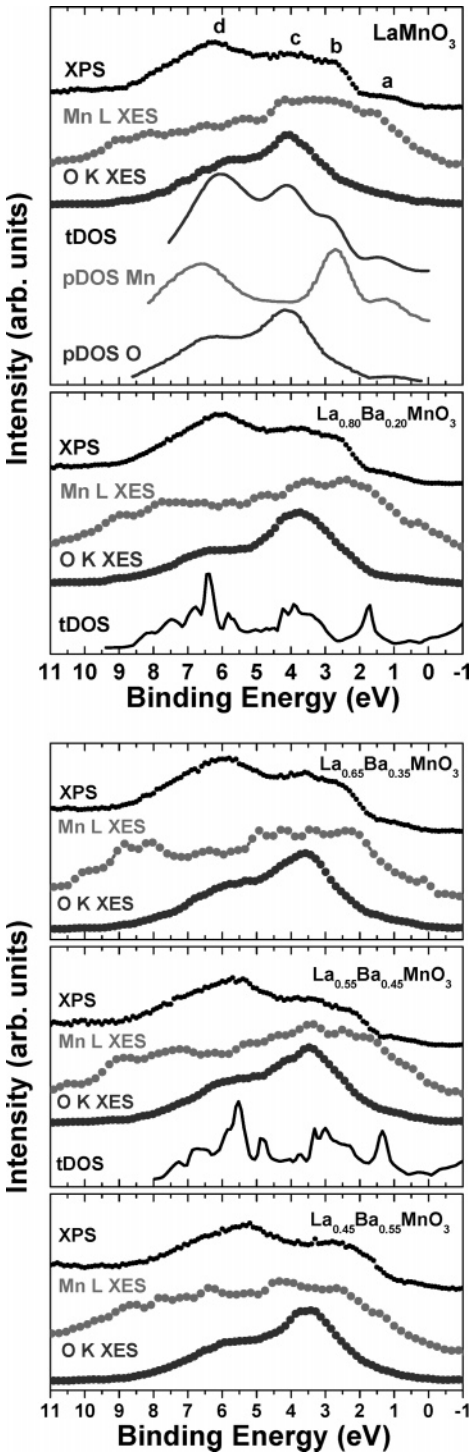

Figure 1. XPS valence band and XES spectra of the Mn 2p and the O 1s edge (plotted on a binding energy scale using the XPS core level binding energies) of $La_{1-x}Ba_xMnO_3$ ($0.0 \le x \le 0.55$). For $LaMnO_3$, $La_{0.8}Ba_{0.2}MnO_3$, and $La_{0.55}Ba_{0.45}MnO_3$ the experimental data are compared with the results of theoretical band structure calculations (labeled (tDOS) and (pDOS), respectively). The calculated data for $LaMnO_3$ have been extracted from Ravindran et al.,[22] whereas the values for the Ba-doped compounds have been taken from Youn et al.[21]

The valence band region of these materials consists, as for $La_{1-x}Ba_xMnO_3$, of four distinct bands (*a*−*d*) spanning the energy range from E_F to about 11 eV. However, the intensity ratios of bands *a*−*c* in the valence bands of the Mn-site-doped samples show significant differences compared to $La_{0.75}Ba_{0.25}MnO_3$. The valence band of $La_{0.76}Ba_{0.24}Mn_{0.84}Co_{0.16}O_3$ shows higher intensities for bands *a*−*c* compared to the reference spectrum, while

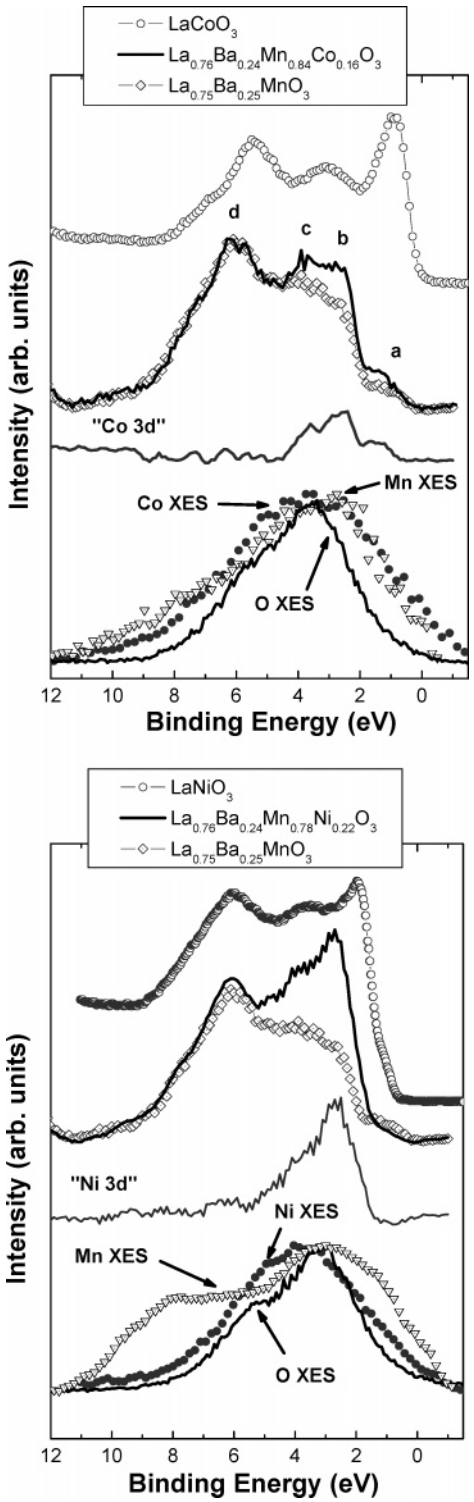

Figure 2. XPS valence band and corresponding XES data of $La_{0.76}Ba_{0.24}Mn_{0.84}Co_{0.16}O_3$ (upper panel) and $La_{0.76}Ba_{0.24}Mn_{0.78}Ni_{0.22}O_3$ (lower panel) plotted an a binding energy scale. For comparison, also the XPS valence band of $La_{0.75}Ba_{0.25}MnO_3$ has been normalized to the Ba 5p XPS peak. The subtraction of the two spectra leads to a representation of the Co 3d and the Ni 3d contributions to the valence band of the corresponding sample. The XPS valence bands of $LaCoO_3$ and $LaNiO_3$ are also shown for comparison.

feature *d* is of approximately the same intensity in both spectra. In Figure 2 we present also a difference spectrum of the valence spectra of $La_{0.76}Ba_{0.24}Mn_{0.84}Co_{0.16}O_3$ and $La_{0.75}Ba_{0.25}MnO_3$, which can be associated, to a large extent, with the Co 3d contribution to the Co-doped sample. The high intensity of band *a* in the Co-doped compound is a clear indication of the presence of Co 3d e_g states near E_F, whereas the Co 3d t_{2g} states probably mainly contribute to features *b* and *c* over an energy range of 2−4.5 eV on a binding energy scale. A more detailed discussion with respect to the Co concentration dependence in this kind of material can be found elsewhere.[17] The XPS valence band of $La_{0.76}Ba_{0.24}Mn_{0.84}Co_{0.16}O_3$ is also compared with the Mn 2p, Co 2p, and O 1s XES measurements. As for $La_{1-x}Ba_xMnO_3$, the XES experiment reveals strongly overlapping Mn 3d and O 2p densities over the whole valence band region. The Co 3d → 2p XES also suggests hybridization and charge transfer between Co 3d and O 2p bands over a large region of the valence band.

In the case of $La_{0.76}Ba_{0.24}Mn_{0.78}Ni_{0.22}O_3$, band *a* shows a significantly lower intensity compared to that of $La_{0.75}Ba_{0.25}MnO_3$, suggesting a lower occupation of the e_g states around E_F. Features *b* and *c* are much more pronounced for the Ni-doped compound. Finally, band *d* has the same intensity for both compounds. We also derived the difference spectrum between the valence band spectra of the Ni-doped compound and $La_{0.75}Ba_{0.25}MnO_3$, where the difference reflects the Ni 3d contributions to the valence band of $La_{0.76}Ba_{0.24}Mn_{0.78}Ni_{0.22}O_3$. The difference spectrum suggests a large contribution of Ni 3d states, spanning the energy range of around 1.5−5 eV. Also, the comparison with the XPS valence spectrum of $LaNiO_3$ confirms that the Ni 3d states contribute to the valence band at lower binding energies than the Mn 3d states, except the e_g levels near E_F of the Mn compound, which is not present for Ni. The Mn 2p and O 1s XES spectra again indicate strong hybridzation effects between Mn 3d → 2p and O 2p → 1s, spanning the energy range from 1 to ∼9 eV. Also, the Ni 2p XES, which reaches its maximum intensity at around 3.5 eV, suggests a significant overlapping with O 2p states, mainly between 2 and 7 eV.

3.2. XAS and RIXS. In Figure 3, we present the XAS spectra of the Mn $L_{2,3}$ edge and the O K edge of $LaMnO_3$. The Mn $L_{2,3}$ XAS spectra, which are dominated by transitions to Mn 3d states but also contain contributions from Mn 4s states, consist of two broad multiplets due to the spin−orbit splitting of the Mn 2p core hole. The 2p edge XAS spectra of TM oxides can be understood in the framework of atomic multiplet theory,[39] since the XAS structures are affected by the core hole wave function. The Mn 2p XAS spectra (Figure 3) can be compared with ligand-field multiplet calculations for Mn^{3+} in D_{4h} crystal symmetry.[40] However, excellent agreement is achieved with recently reported model calculations based upon a $(MnO_6)^{10-}$ charge-transfer cluster model in D_{4h} symmetry.[36] Following the argumentation of Taguchi et al., the ground state can be described as a superposition of 73.6% $3d^4$ states and 26.4% $3d^5$ L charge-transfer states. Hole doping with Ba leads to a change of the chemical environment and consequently to a chemical shift of the maxima of the Mn L_3 edge toward higher photon energies, as has been previously observed for $La_{1-x}Sr_xMnO_3$.[41]

In the case of XAS on the ligand K edge the situation is different. The O K edge spectra are dominated by transitions to O 2p states hybridized with Mn 3d states and Mn 4s contributions.[22] The spectra consist of two features, the first of which is located at photon energies around 528 eV while the second one is a broad feature between 531 and 535 eV. For $LaMnO_3$ we find that two prominent peaks are present in the low-energy feature. This result can be described accurately with single-particle calculations.[22] Doping with Ba leads to a change of the spectral shape, and the double peak structure at both features disappears. The first feature, which shows a slight shift toward lower photon energies with increasing *x*, has been

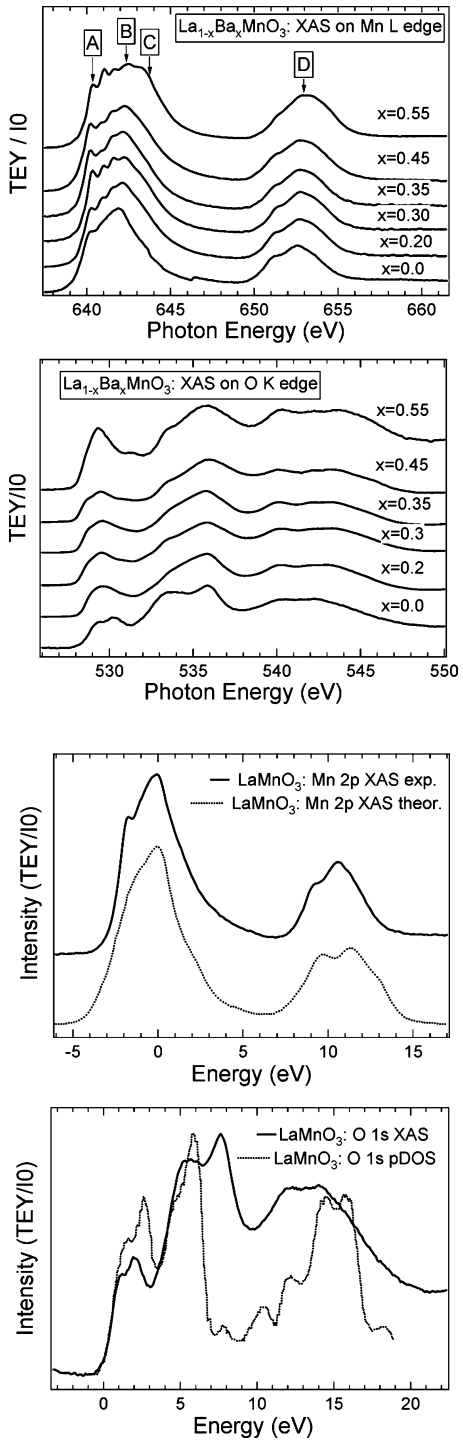

Figure 3. Upper panel: XAS spectra of the Mn L edge (upper panel) and the O K edge of $La_{1-x}Ba_xMnO_3$ ($0.2 \leq x \leq 0.55$). The data are recorded in total electron yield (TEY) mode. Labels A−D indicate the excitation energies of the RIXS spectra recorded at the Mn L edge (see Figure 4). Lower panel: Mn $L_{2,3}$ and O K (lower panel) XAS regions of $LaMnO_3$, brought to a common energy scale with theoretical calculations: The Mn 2p XAS multiplet calculation has been adapted from Taguchi et al.,[36] and the O K XAS is compared with a LDA+U calculation from Wessely et al.[35]

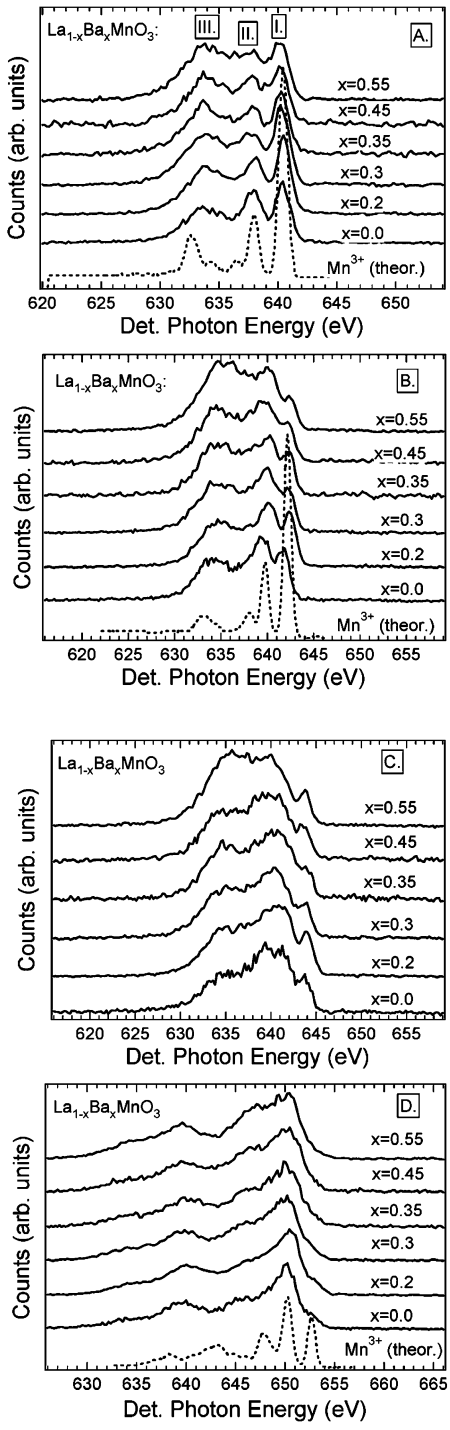

Figure 4. Mn L_3 resonant inelastic X-ray scattering spectra of $La_{1-x}Ba_xMnO_3$ ($0.0 \leq x \leq 0.55$) recorded at different excitation energies near the Mn L_3 edge. The excitation energies are those labeled A−D in the XAS spectra (Figure 3): A, 640.2 eV; B, 641.8 eV; C, 643.8 eV; D, 652.7 eV. The RIXS spectra consist of three main features labeled I−III (see text). The dashed lines represent multiplet calculations performed for Mn^{3+} ions.[30]

attributed by Youn et al.[21] to O 2p states hybridized with Mn 3d states, whereas the second broad structure is due to O 2p states hybridized with La 5d states.

Figure 4 shows the RIXS spectra taken at the Mn L_3 edges of $La_{1-x}Ba_xMnO_3$ ($0.2 \leq x \leq 0.55$), and Figure 4 displays the RIXS results recorded at the Mn $L_{2,3}$ edge; labels A−D correspond to the excitation energies as marked in the XAS spectrum (Figure 3). At each composition the spectra have been normalized with respect to the height elastic recombination peak. The RIXS spectra depend strongly on the incident photon energy and Ba concentration. The emission spectra corresponding to excitation energies A and B consist of three main resonant features labeled I−III. Feature I can be associated with the elastic recombination peak whereas features II and III represent resonant loss features, which appear at constant energy with respect to the elastic recombination peak. In the case of peak II

a fixed energy loss of around 2.5 eV below the elastic peak is observed while peak III is a rather broad structure 6−9 eV below the recombination peak. At higher excitation energies above the Mn L_3 threshold (C) the emission spectra contain more nonresonant features which contribute to the spectra as dispersing features. If the excitation energy is increased to the Mn L_2 edge, the elastic peak almost disappears while the loss feature located 2.5 eV below the recombination peak shows a strong resonance. Also, the second loss feature appears, while one can observe normal emission due to transitions from the Mn 3d states to the Mn $2p_{3/2}$ level (Figure 4). One can now identify the features with the help of the results shown above. The XPS spectra (Figure 1) show a sharp increase in intensity with a maximum at 2.5 eV (peak *b*) on a binding energy scale which is due to more or less localized (dependent on hole concentration) Mn t_{2g} states of the majority spin band. Hence, loss feature II may be associated with intraatomic Mn d−d transitions between occupied and unoccupied Mn 3d bands. Taking the XPS and XES results (section 3.1), feature III can be attributed to charge-transfer excitations from the occupied Mn 3d e_g and t_{2g} bands hybridized with O 2p states to the Mn e_g states in the conduction band. With increasing hole concentration x the intensity of the charge-transfer feature (III) increases. This finding is consistent for the RIXS spectra labeled A and B, and furthermore it can also be seen from the spectra recorded with excitation energies above the Mn L_3 edge (C) that the intensity of emission features corresponding to interatomic transitions increases with increased hole doping. The spectra taken at excitation energy D on the maximum of L_2 absorption show an intensity ratio of L_α to L_β of about 0.5. This is consistent with the results of Yablonskikh et al.[42] on Mn-based Heusler alloys, where it was found that magnetic ordering decreases the L_α/L_β branching ratio, with respect to nonmagnetic structures. Also, the multiplet calculations[30] (Figure 4) reproduce the RIXS spectra of $LaMnO_3$ rather well. Features II and III can be described as local d−d transitions and O 2p → Mn 3d charge-transfer excitations. A more detailed discussion can be found in section 4.

4. Discussion

The XPS valence bands of $La_{1-x}Ba_xMnO_3$ ($0 < x < 0.55$) (Figure 1) consist of four distinct regions. A weak feature is due to Mn e_g states near E_F, followed by a sharp increase in intensity around 2.5 eV binding energy, which is attributed to localized Mn t_{2g} states. The spectra reveal a broadening of the Mn t_{2g} states in the valence band with higher Ba concentration. This finding is consistent with recent band structure calculations.[21,22] The O Kα XES maximum intensities (Figure 1) show a shift toward E_F (from ∼4.5 to ∼3.5 eV) with higher doping concentration. This places the oxygen and Mn states closer in energy, and hence hybridization between the Mn t_{2g} states and O 2p states in the valence band is expected to be stronger with higher Ba concentration.

Features *a*−*c* of the XPS valence band of $La_{0.76}Ba_{0.24}Mn_{0.84}Co_{0.16}O_3$ show a significantly higher intensity. The Co contributes to band *a* with 3d e_g like states and bands *b* and *c* with 3d t_{2g} like states. In contrast to the trivalent Co ions in $LaCoO_3$ (XPS valence spectrum also shown in Figure 2), the divalent Co ions in this compounds are not in a low-spin state but have a nonzero magnetic moment, inducing also a negative $Co^{2+}-O-Mn^{4+}$ superexchange interaction. The Co 2p XES spectrum is in reasonable agreement with this result, but it indicates a somewhat broader contribution of Co 3d states between 1 and 8 eV on a binding energy scale. According to theory,[43] some Co 3d states are also present around 5−7 eV, hybridized with O 2p states, which contribute to the Co 3d → 2p XES spectrum. Furthermore, the XES spectrum is influenced by lifetime broadening effects. The Mn 3d → 2p and O 2p → 1s XES spectra lead to results similar to $La_{1-x}Ba_xMnO_3$. This is also the case for $La_{0.76}Ba_{0.24}Mn_{0.78}Ni_{0.22}O_3$, whereas the Ni 3d → 2p XES experiment suggests the presence of Ni 3d states from about 1.5 to 7 eV. This is in reasonable agreement with the "Ni 3d" difference spectrum (Figure 2) which indicates that Ni 3d states contribute to the valence band in a region of 1.5−5 eV. In comparison with the XPS valence band $LaNiO_3$ and band structure calculations for $LaNiO_3$ [44] and $LaMn_{1-x}Ni_xO_3$, [45] one can draw the conclusion that the Ni 3d states in this kind of compound are more localized than Mn 3d states and lead to a weaker occupancy of e_g-like states near E_F. Magnetic measurements for this specific compound are not known to us. However, experiments on other manganites have shown that Ni doping at the Mn site induces a metal−insulator transition at low concentrations, a few percent, but also leads to a decrease of Curie temperature and magnetic moment at higher concentrations.[14,45] The lowering of the e_g state occupancy as well as the weaker interaction of the Ni 3d states with the O 2p states in the valence band region suggests that one may find similar magnetic properties for $La_{0.76}Ba_{0.24}Mn_{0.78}Ni_{0.22}O_3$. In contrast, Co-doping leads to a stronger occupancy of the e_g-like states near E_F, which may be an explanation for the intricate magnetic transport properties, resulting in sharp magnetoresistance maxima in $La_{0.74}Ba_{0.26}Mn_{1-y}Co_yO_3$ around a Co concentration of $y = 0.16$. On the other hand, the interaction of the divalent Co ions and Mn^{4+} ions may lead to a decrease of the Curie temperature in these compounds.[15]

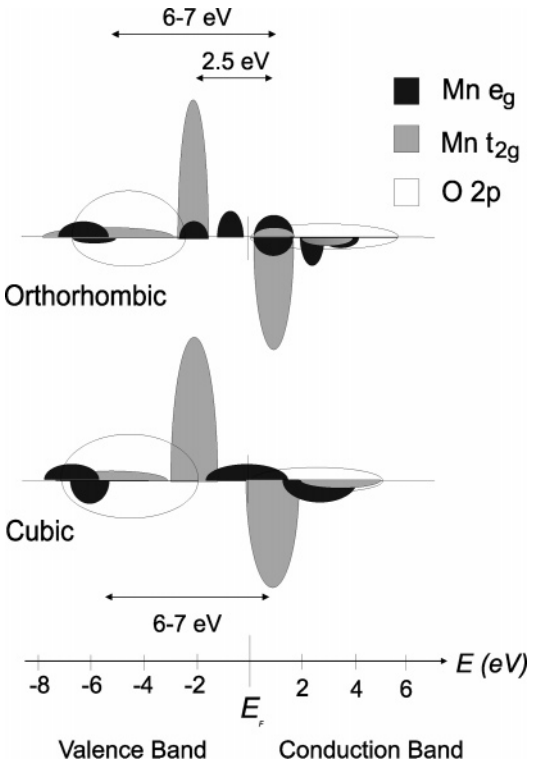

Figure 5. Schematic plot of the partial densities of states of O 2p and Mn 3d for the orthorhombic $GdFeO_3$ structure (upper panel) and the cubic perovskite-type structure. Densities above the energy axis are majority spin states, and those below are minority spin states. The values are based upon our experimental findings and the calculations of Ravindran et al.[22] and Youn et al.,[21] respectively.

In Figure 5, we present a schematic plot of the partial densities of Mn 3d and O 2p states for the orthorhombic crystal structure

of undoped $LaMnO_3$ and the cubic perovskite structure, which is found for highly doped $La_{1-x}Ba_xMnO_3$ ($x > 0.35$).[9] For the orthorhombic phase, an energy gap between the highest occupied Mn e_g band (spin up) and the lowest unoccupied Mn e_g band (unpolarized) is found, followed by a localized band comprising Mn t_{2g} states (spin up) around 2 eV which is mixed with some Mn e_g derived states. At higher binding energies (~3−9 eV) the valence band comprises mainly unpolarized O 2p states hybridized with some Mn 3d states. For the cubic crystal structure the gap between the Mn e_g bands near E_F closes and the compound becomes metallic. The Mn t_{2g} states are still more or less localized. However, they contribute to a broader region of the valence band (~1−3 eV binding energy) compared to the orthorhombic structure. Furthermore, O K XES data reveal a stronger hybridization between Mn t_{2g} and O 2p bands while theory predicts almost no overlap between Mn t_{2g} and Mn e_g bands in the valence band.

A preliminary interpretation of the RIXS spectra at the Mn L edge of $La_{1-x}Ba_xMnO_3$ is possible by considering the XPS, XES, and band theory.[31,34] RIXS spectra recorded at excitation energies below and at the Mn L_3 edge (Figure 4) consist of three features. Feature I can be associated with the elastic recombination peak while feature II is due to intraatomic d−d transitions between occupied Mn t_{2g} and unoccupied Mn e_g bands. Finally, feature III can be attributed to interatomic transitions between hybridized O 2p−Mn 3d bands in the valence band and Mn 3d bands in the conduction band.

The selection rules for RIXS (with cubic and orthorhombic symmetry) state that all d−d transitions are allowed: $t_{2g}-t_{2g}$, e_g-e_g, $t_{2g}-e_g$, and e_g-t_{2g}.[27,29] Transitions from occupied Mn e_g states (spin down, hybridized with O 2p) to unoccupied Mn t_{2g} states are likely to make a significant contribution as they have a large density of unoccupied states, making the transition strong, and the energy range in the one-electron picture covers an appropriate range. This is especially the case for the cubic phase (Figure 5) where a significant density of e_g electrons (spin down) is present at a binding energy of around 6 eV due to covalent interaction between Mn e_g and O 2p states.[22] Thus, feature III can be explained as a superposition of a transition between occupied and unoccupied majority states (charge transfer) and minority states (covalent interaction).

The Mn t_{2g}−O 2p hybridization becomes much stronger in cubic symmetry or at higher doping concentration. Consequently, the relative intensity of feature III compared to the intensity of feature II increases. One can now come to the conclusion that hole doping in lanthanum manganites leads to more hybridization between Mn 3d and O 2p bands in the valence band. In RIXS this development can be investigated directly, since the relative intensity of the intraatomic d−d transitions between Mn 3d bands compared to the intensity of the interband transitions of heavily mixed Mn 3d−O 2p bands decreases with increasing hole doping concentration. This finding may support the point of view that the importance of correlation effects has been exaggerated, and furthermore we show that hole doping leads to stronger Mn 3d−O 2p hybridization compared to the undoped compound.

Figure 4 also shows the results of a charge-transfer multiplet calculation of a Mn^{3+} ion in D_{4h} symmetry.[30] Also, within the Anderson impurity model the RIXS loss features of $LaMnO_3$ can be reproduced rather well. The calculated spectra comprise the elastic recombination peak, local d−d transitions located around 2.5 eV below the elastic peak, followed by O 2p → Mn 3d charge-transfer excitations.[30] The 2.5 eV loss feature is rather well reproduced by the multiplet calculation as well as the charge-transfer band. The 2.5 eV loss feature shows a similar behavior and energy position in all samples, showing different magnetic ground states and a metal-to-insulator transition depending on the Ba concentration. This is a rather substantial indication of a local d−d excitation and consequently for the presence of correlation effects. Nonetheless, the 2.5 eV loss peak is also present and even resonating at excitation energy B, corresponding to the maximum of the M L_3 absorption. For this energy and those recorded at higher excitation energies the excitonic states begin to overlap with the ordinary Mn 3d → 2p emission, representing at least parts of the occupied densities of states. This is also the case with increasing doping concentration, since the contribution of the charge-transfer band and transitions between hybridized Mn 3d and O 2p is increasing, leading to an even more extended Mn 3d wave function of the compound in question. To fully understand the Mn 3d → 2p RIXS of $La_{1-x}Ba_xMnO_3$ would require full multiplet calculations for a Mn^{4+} system or even calculations within an extended cluster model. For systems with a not so localized 3d wave function also a simulation of these spectra with the restricted joint DOS (that is a convolution of vacant 3d DOS in a narrow energy interval with the occupied 3d DOS) would be an interesting approach. This is beyond the scope of the present paper. It should be mentioned that both theoretical approaches have been successfully used to describe the Ti 3d → 2p RIXS of TiO_2.[46,47]

5. Conclusions

We have presented a detailed X-ray spectroscopic study of the A-site doped CMR compound $La_{1-x}Ba_xMnO_3$ and the A- and B-site doped manganites $La_{0.76}Ba_{0.24}Mn_{0.84}Co_{0.16}O_3$ and $La_{0.76}Ba_{0.24}Mn_{0.78}Ni_{0.22}O_3$. XPS and XES data reveal hybridization between Mn 3d states and O 2p states in the valence band, and this hybridization becomes stronger with increasing Ba concentration due to the broadening of the Mn t_{2g} states and the shift of the O 2p states toward E_F and thus the Mn t_{2g} states. In $La_{0.76}Ba_{0.24}Mn_{0.84}Co_{0.16}O_3$ the Co 3d states mainly contribute at lower binding energies between 0.5 and 5 eV to the valence band, including the states near E_F. Doping with Ni leads to a lower occupancy of the e_g states near E_F, and the Ni 3d states are rather localized between 1.5 and 5 eV.

The Mn $L_{2,3}$ XAS results of $LaMnO_3$ are in excellent agreement with recent cluster model calculations assuming D_{4h} symmetry.[36] A chemical shift with increasing Ba concentration was observed, indicating the changing chemical environment of Mn. O *K* XAS spectra reveal that hole doping leads to strong mixing of the O 2p−Mn 3d conduction bands and to lower occupation of the O 2p states. This is an indication for the O 2p character of holes in mixed valent manganites, a view which is supported by other studies based upon EELS[48] and Mn 3s core level photoemission spectroscopy.[49]

RIXS spectra, which have been performed at the Mn L edge, consist of three main features, which can be associated with the elastic recombination peak and two loss features. The peak located around 2.5 eV below the elastic peak can be associated with a local Mn d−d transition, in agreement with multiplet calculations, and the second feature can be assigned to charge-transfer transitions. Since the loss features remain present at excitation energies at the Mn $L_{2,3}$ XAS maxima, they represent parts of the joint DOS, with the states projected on the Mn site. With increasing Ba concentration the hybridization between O 2p and Mn t_{2g} bands in the valence band becomes stronger, which can be directly investigated by RIXS: the intensity of the corresponding peak increases with increasing Ba concentra-

tion. In summary, we have shown that colossal magnetoresistance manganites can be understood as being moderately correlated systems, in which hybridization effects like charge transfer and also covalent interaction between the Mn and O states for both occupied and unoccupied states may play an important role with respect to their unusual phenomena and transport properties.

Acknowledgment. Financial support of the PhD program of Lower Saxony and DFG, especially Graduiertenkolleg, is gratefully acknowledged. This work was partly supported by the Russian Foundation for Basic Research (Grant 04-03-96092-Ural) and the Research Council of President of Russian Federation (Project NSH-1026.2003.2). The Advanced Light Source at LBNL is supported by DOE Contract DE-A003-76SF00098. The ROSA spectrometer is partly supported by BMBF Project no. 05 SR8 OL1-2. J. D. Denlinger is acknowledged for excellent technical support. We are grateful to A. V. Postnikov and S. Bartkowski for informative and helpful discussions.

References and Notes

(1) Millis, A. J. *Nature (London)* **1998**, *392*, 147.
(2) Salamon, M. B.; Jaime, M. *Rev. Mod. Phys.* **2001**, *73*, 583.
(3) Chuang, Y. D.; Gromko, A. D.; Dessau, D. S.; Kimura, T.; Tokura, Y. *Science* **2001**, *292*, 1509.
(4) von Helmolt, R.; Wecker, J.; Holzapfel, B.; Schultz, L.; Samwer, K. *Phys. Rev. Lett.* **1993**, *71*, 2331.
(5) Jin, S.; Tiefel, T. H.; McCormack, M.; Fastnacht, R. A.; Ramesh, R.; Chen, L. H. *Science* **1994**, *264*, 413.
(6) Pickett, W. E.; Moodera, J. S. *Phys. Today* **2001**, *54*, 39.
(7) Park, J. H.; Vescovo, E.; Kim, H. J.; Kwon, C.; Ramesh, R.; Venkatesan, T. *Nature (London)* **1998**, *392*, 794.
(8) Ju, H. L.; Nam, Y. S.; Lee, J. E.; Shin, H. S. *J. Magn. Magn. Mater.* **2000**, *219*, 1.
(9) Dabrowski, B.; Rogacki, K.; Xiong, X.; Klamut, P. W.; Dybzinski, R.; Shaffer, J.; Jorgensen, J. D. *Phys. Rev. B* **1998**, *58*, 2716.
(10) Roy, C.; Budhani, R. C. *J. Appl. Phys.* **1999**, *85*, 3124.
(11) Murugavel, P.; Lee, J. H.; Yoon, J. G.; Noh, T. W.; Chung, J. S.; Heu, M.; Yoon, S. *Appl. Phys. Lett.* **2003**, *82*, 587.
(12) Mandal, P.; Ghosh, B. *Phys. Rev. B* **2003**, *68*, 014422.
(13) Chatterji, T.; Regnault, L. P.; Schmidt, W. *Phys. Rev. B* **2002**, *66*, 214408.
(14) Maignan, A.; Damay, F.; Barnabe, A.; Martin, C.; Hervieu, M.; Raveau, B. *Philos. Trans. R. Soc. A* **1998**, *356*, 1635.
(15) Khalyavin, D. D.; Pekala, M.; Bychkov, G. I.; Shiryaev, S. V.; Barilo, S. N.; Troyanchuk, I. O.; Mucha, J.; Misiorek.; Szymczak, R.; Baran, M.; Szymczak, H. *J. Phys.: Condens. Matter* **2003**, *15*, 925.
(16) Demeter, M.; Neumann, M.; Galakhov, V. R.; Ovechkina, N. A.; Kurmaev, E. Z.; Labachevskaya, N. I. *Acta Phys. Pol., A* **2000**, *98*, 587.
(17) Falub, M. C.; Tsurkan, V.; Neumann, M.; Troyanchuk, I. O.; Galakhov, V. R.; Kurmaev, E. Z.; Weitering, H. H. *Surf. Sci.* **2003**, *532*−*535*, 488.
(18) Park, J. H.; Chen, C. T.; Cheong, S. W.; Bao, W.; Meigs, G.; Chakarian, V.; Idzerda, Y. U. *Phys. Rev. Lett.* **1996**, *76*, 4215.
(19) Saitoh, T.; Bocquet, A. E.; Mizokawa, T.; Namatame, H.; Fujimori, A.; Abbate, M.; Takeda, Y.; Takano, M. *Phys. Rev. B* **1995**, *51*, 13942.
(20) Hamada, N.; Sawada, H.; Terakura, K. *J. Phys. Chem. Solids* **1995**, *56*, 1719.
(21) Youn, S. J.; Min, B. I. *Phys. Rev. B* **1997**, *56*, 12046.
(22) Ravindran, P.; Kjekshus, A.; Fjellvåg, H.; Delin, A.; Eriksson, O. *Phys. Rev. B* **2002**, *65*, 064445.
(23) Carlisle, J. A.; Shirley, E. L.; Hudson, E. A.; Terminello, L. J.; Callcott, T. A.; Jia, J. J.; Ederer, D. L.; C.Perera, R. C.; Himpsel, F. J. *Phys. Rev. Lett.* **1995**, *74*, 1234.
(24) Kotani, A.; Shin, S. *Rev. Mod. Phys.* **2001**, *73*, 203.
(25) Kramers, H. A.; Heisenberg, W. *Z. Phys.* **1925**, *31*, 681.
(26) Materlik, G., Sparks, C. J., Fischer, K., Eds.; *Resonant Anomalous X-ray Scattering*; Elsevier Science B.V.: Amsterdam, 1994.
(27) Butorin, S. M.; Guo, J.-H.; Magnuson, M.; Kuiper, P.; Nordgren, J. *Phys. Rev. B* **1996**, *54*, 4405.
(28) Duda, L. C.; Nordgren, J.; Dräger, G.; Bocharov, S.; Kirchner, T. *J. Electron. Spectrosc. Relat. Phenom.* **2000**, *110*−*111*, 275.
(29) Zhang, G. P.; Callcott, T. A.; Woods, G. T.; Lini, L.; Sales, B.; Mandrus, D.; He, J. *Phys. Rev. Lett.* **2002**, *88*, 077401.
(30) Butorin, S. M.; Såthe, C.; Saalem, F.; Nordgren, J.; Zhu, X.-M. *Surf. Rev. Lett.* **2002**, *9*, 989.
(31) Kurmaev, E. Z.; Korotin, M. A.; Galakhov, V. R.; Finkelstein, L. D.; Zabolotzky, E. I.; Erfremova, N. N.; Lobachevskaya, N. I.; Stadler, S.; Ederer, D. L.; Callcott, T. A.; Zhou, L.; Moewes, A.; Bartkowski, S.; Neumann, M.; Matsuno, J.; Mizokawa, T.; Fujimori, A.; Mitchell, J. *Phys. Rev. B* **1999**, *59*, 12799.
(32) Duda, L.-C. *J. Electron. Electron. Spectrosc.* **2000**, *110*−*111*, 287.
(33) Prince, K. C.; Kuepper, K.; Neumann, M.; Cocco, D.; Bondino, F.; Zangrando, M.; Zacchigna, M.; Matteucci, M.; Parmigiani, F. *J. Phys.: Condens. Matter* **2004**, *16*, 7397.
(34) Bondino, F.; Platé, M.; Zangrando, M.; Cocco, D.; Comin, A.; Alessandri, I.; Malavasi, L.; Parmigiani, F. *J. Phys. Chem. B* **2004**, *108*, 4018.
(35) Wessely, O.; Roy, P.; Åberg, D.; Andersson, C.; Edvardsson, S.; Karis, O.; Sanyal, B.; Svedlindh, P.; Katsnelson, M. I.; Gunnarsson, R.; Arvanitis, D.; Eriksson, O. *Phys. Rev. B* **2003**, *68*, 235109.
(36) Taguchi, M.; Altarelli, M. *Surf. Rev. Lett.* **2002**, *9*, 1167.
(37) Jia, J. J.; Calcott, T. A.; Yurkas, J.; Ellis, A. W.; Himpsel, F. J.; Samant, M. G.; Stöhr, G.; Ederer, D. L.; Carlisle, J. A.; Hudson, E. A.; Terminello, L. J.; Shuh, D. K.; Perera, R. C. C. *Rev. Sci. Instrum.* **1995**, *66*, 1394.
(38) Chastain, J. *Handbook of X-ray Photoelectron Spectroscopy*; Perkin-Elmer Corp.: Eden Prairie, MN, 1992.
(39) Cowan, R. D. *The Theory of Atomic Structure and Spectra*; University of California Press: Berkeley, CA, 1981.
(40) Castleton, C. W. M.; Altarelli, M. *Phys. Rev. B* **2000**, *62*, 1033.
(41) Abbate, M.; de Groot, F. M. F.; Fuggle, J. C.; Fujimori, A.; Strebel, O.; Lopez, F.; Domke, M.; Kaindl, G.; Sawatzky, G. A.; Takana, M.; Takeda, Y.; Eisaki, H.; Uchida, S. *Phys. Rev. B* **1992**, *46*, 4511.
(42) Yablonskikh, M. V.; Yarmoshenko, Y. M.; Gerasimov, E. G.; Gaviko, V. S.; Korotin, M. A.; Kurmaev, E. Z.; Bartkowski, S.; Neumann, M. *J. Magn. Magn. Mater.* **2002**, *256*, 396.
(43) Yang, Z.; Yie, L.; Xie, X. *Phys. Rev. B* **1999**, *59*, 7051.
(44) Solovyev, I.; Hamada, N.; Terakura, K. *Phys. Rev. B* **1996**, *53*, 7158.
(45) Yang, Z. Q.; Ye, L.; Xie, X. D. *Phys. Status Solidi B* **2000**, *220*, 885.
(46) Finkelstein, L. D.; Kurmaev, E. Z.; Korotin, M. A.; Moewes, A.; Schneider, B.; Butorin, S. M.; Guo, J.-H.; Nordgren, J.; Hartmann, D.; Neumann, M.; Ederer, D. L. *Phys. Rev. B* **1999**, *60*, 2212.
(47) Kotani, A. *J. Electron. Spectrosc. Relat. Phenom.* **2000**, *110*−*111*, 197.
(48) Ju, H. L.; Sohn, H. C.; Krishnan, K. M. *Phys. Rev. Lett.* **1997**, *79*, 3230.
(49) Galakhov, V. R.; Demeter, M.; Bartkowski, S.; Neumann, M.; Ovechkina, N. A.; Kurmaev, E. Z.; Lobachevskaya, N. I.; Mukovskii, Y. M.; Mitchell, J.; Ederer, D. L. *Phys. Rev. B* **2002**, *65*, 113102.